A simple approach for designing quad-band rat-race couplers using modified T-shaped structures

Nguyen Minh Giang (ID), Le Ho Manh Thang and Tran Thi Thu Huong

Faculty of Radio-Electronic Engineering, Le Quy Don Technical University, Hanoi, VietNam
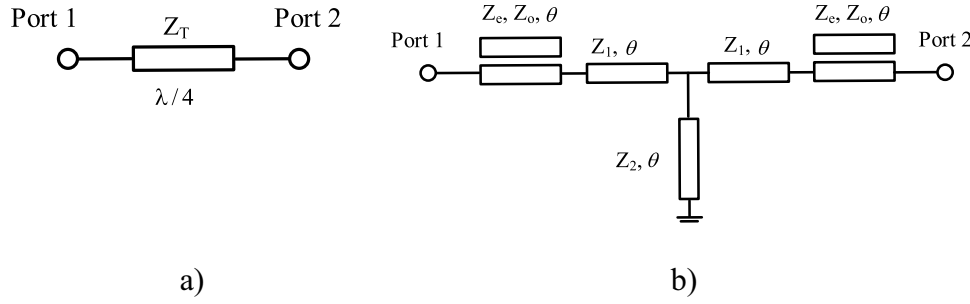
Abstract

This paper presents a novel design of quad-band rat-race couplers (RRCs) based on a modified T-shaped structure (MTSS). Two coupled lines are incorporated into the conventional dual-band T-shaped structure to create the MTSS, making it equivalent to a quarter-wavelength transmission line at four operating bands. The ABCD matrix method is applied to analyze the quad-band MTSS, deriving closed-form equations for calculating parameters of the structure. Then, a conventional RRC is separated into quarter-wavelength transmission lines, which are replaced by the proposed MTSS. To validate the design method, a quad-band RRC operating at 0.6, 1.196, 1.853, and 2.45 GHz is designed, fabricated, and tested. Simulation and experimental results demonstrate excellent agreement with theoretical prediction. The measured results show that input return loss exceeds 21.75 dB, isolation is greater than 21.6 dB, and insertion loss is less than 4.4 dB at all four operating frequencies. Phase deviations observed from the measured in-phase and out-phase responses are within $0° ± 4.6°$ and $180° ± 6.7°$, respectively. Compared to most previously reported quad-band RRCs, the proposed circuit features a simple design and offers superior performance in isolation, return loss, and insertion loss.

Introduction

Rat-race couplers (RRCs) are crucial components in communication systems. They are extensively utilized in a variety of microwave circuits, such as balanced power amplifiers, phase shifters, data modulators, and mixers. Many studies have focused on improving some features of the RRCs, such as enhanced bandpass characteristics [1–3], reduced size [4, 5], harmonic suppression [6, 7], and a high power division ratio [8, 9]. Otherwise, to improve the performance of the system in terms of high capacity, multi-task, and compact size, it requires that the system can operate with different frequencies. Hence, the requirement for the design of multi-band components has become more and more essential. The RRCs were investigated to work in multi-band, such as dual-band, tri-band, and quad-band. To design the dual-band RRCs, the researchers have introduced several structures including Pi-shaped configurations [10, 11], T-shaped structures [12, 13], step-impedance sections [14], and synthetic transmission lines [15] to replace quarter-wavelength transmission lines in the conventional RRCs. Tri-band RRCs were designed using various techniques. In [16], a tri-band Pi-shaped structure incorporating resonators was proposed, while [17] employed a T-shaped step-impedance transformer to achieve tri-band performance. Notably, three operating frequencies in the work [17] are not completely independent since the middle frequency is an average of the upper and lower frequencies. Another method is the application of metamaterial in [18], but this type causes complexity in analysis and fabrication.

In recent years, with the advancement of quad-band applications, various quad-band circuits have been studied, such as quad-band filters [19, 20], quad-band antennas [21, 22], and quad-band power amplifiers [23]. However, research on quad-band RRCs remains limited. To the best of the author's knowledge, only studies [24], [25], and [26] have addressed these issues so far. In [24], a quad-band RRC was designed using a Pi-shaped quad-band microstrip line. However, its frequency ratio of the largest to the smallest operating frequency is restricted to 4.5, as shown in [27], where the same quad-band structure was used in a Wilkinson power divider. Since both designs are based on replacing the 70.71-ohm quarter-wavelength transmission line with the same Pi-shaped quad-band structure, they share the same frequency ratio limitation, making them less suitable for wideband applications. The study in [25] introduced a quad-band RRC designed with negative-refractive-index transmission lines and incorporating MIM capacitors and chip inductors. However, the quad-band RRC [25] exhibits limitations in terms of low isolation and poor insertion loss. A quad-band RRC with spurious pass-band suppression was introduced in [26]. This design used a laterally offset dual ring (LODR) resonator backed with concentric dual split ring (CDSR) slots. It is observed that this quad-band RRC

CAMBRIDGE
UNIVERSITY PRESS

Figure 1. (a) A quarter-wavelength transmission line. (b) A proposed modified T-shape structure.

has the disadvantages of a high insertion loss and significant phase deviation. Thus, some problems obtained in the previous quad-band RRCs need to be solved to achieve high performance.

This paper presents a novel and simple design of a quad-band RRC based on a proposed modified T-shaped structure (MTSS). Two coupled lines are integrated into the conventional dual-band T-shaped structure to form the MTSS. The MTSS are then employed to replace the quarter-wavelength transmission lines in the conventional RRC. Compared to previously reported quad-band RRCs [25, 26], which rely on negative refractive index transmission lines with lumped components [25] or complex two-layer structures [26], the proposed quad-band RRC employs a simpler design approach. It features a planar structure without any lumped elements. The closed-form design equations for the proposed structure are derived through analytical methods. Moreover, a detailed analysis of the design constraints is provided, demonstrating that the proposed quad-band RRC can achieve a frequency ratio between the highest and lowest operating frequencies not exceeding 5.39. To evaluate the effectiveness of the design method, a prototype of quad-band RRC operating at 0.6, 1.196, 1.853, and 2.45 GHz was designed, fabricated, and tested. Good agreement between the simulation and measurement results validates the feasibility of the proposed approach. The measured results show that at the four operating frequencies, the proposed quad-band RRC exhibits an insertion loss of less than 4.4 dB, while simultaneously achieving a return loss exceeding 21.75 dB and an isolation level greater than 21.6 dB.

Model and formulation of the proposed MTSS

The proposed MTSS is presented in Fig. 1(b). This MTSS is equivalent to a quarter-wavelength transmission line with a characteristic impedance of Z_T (Fig. 1a) at four operating bands. The proposed MTSS is developed by adding two series coupled lines to the conventional dual-band T-shaped structure [28]. The MTSS is composed of two transmission lines, two coupled lines, and a short stub. Two transmission lines are the same with characteristic impedance Z_1 and electrical length θ. Two coupled lines have the same even and odd characteristic impedances (Z_e and Z_o) and the same electrical length θ. The short stub has characteristic impedance Z_2 and electrical length θ.

To determine the parameters of the proposed MTSS, the methodology from [24] was applied. The ABCD matrix of the proposed MTSS is the product of ABCD matrices of sections:

$$M = \begin{bmatrix} A & B \\ C & D \end{bmatrix} = M_C M_1 M_2 M_1 M_C \tag{1}$$

In which, M_C, M_1, and M_2 are ABCD matrices of coupled line, transmission line (Z_1, θ), and short stub (Z_2, θ), respectively. These matrices are determined as follows:

$$M_C = \begin{bmatrix} \cos\theta & \frac{j(Z_e+Z_o)\sin\theta}{2} \\ \frac{j2\sin\theta}{(Z_e+Z_o)} & \cos\theta \end{bmatrix} \tag{2}$$

$$M_1 = \begin{bmatrix} \cos\theta & jZ_1\sin\theta \\ \frac{j\sin\theta}{Z_1} & \cos\theta \end{bmatrix} \tag{3}$$

$$M_2 = \begin{bmatrix} 1 & 0 \\ -\frac{j\cot\theta}{Z_2} & 1 \end{bmatrix} \tag{4}$$

Besides, the ABCD matrix of the quarter-wavelength transmission line with characteristics impedance Z_T has the following form:

$$M_T = \begin{bmatrix} 0 & jZ_T \\ \frac{j}{Z_T} & 0 \end{bmatrix} \tag{5}$$

To make the proposed MTSS equivalent to the quarter-wavelength transmission line, the following relation must be satisfied:
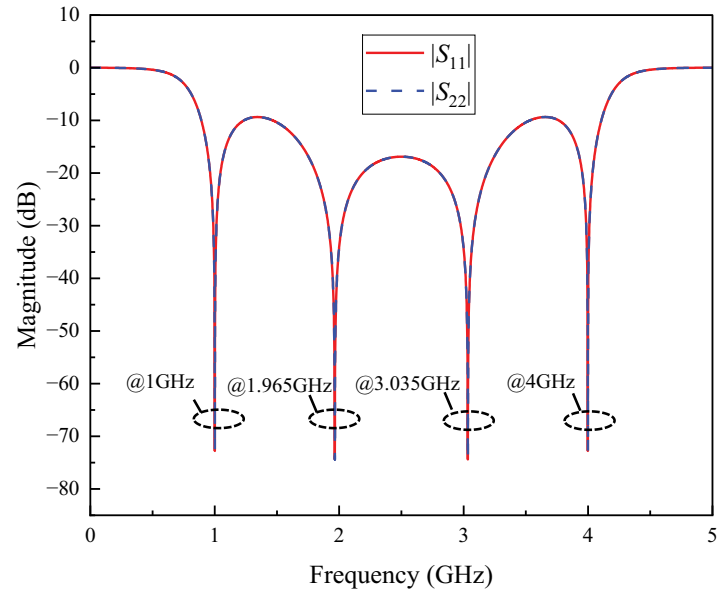
$$M_C M_1 M_2 M_1 M_C = \pm M_T \tag{6}$$

Hence,

$$M_1 M_2 M_1 = \pm M_C^{-1} M_T M_C^{-1} \tag{7}$$

By substituting Equations (2)–(4) and (5) into Equation (7), the following equation is obtained:

$$\begin{bmatrix} \left(1+\frac{Z_1}{Z_2}\right)\cos^2\theta - \sin^2\theta & j\left(Z_1+\frac{Z_1^2}{2Z_2}\right)\sin 2\theta \\ j\left(\frac{\sin 2\theta}{Z_1} - \frac{\cos^2\theta\cot\theta}{Z_2}\right) & \left(1+\frac{Z_1}{Z_2}\right)\cos^2\theta - \sin^2\theta \end{bmatrix}$$
$$= \pm \begin{bmatrix} \left(\frac{Z_C}{4Z_T}+\frac{Z_T}{Z_C}\right)\sin 2\theta & j\left(Z_T\cos^2\theta - \frac{Z_C^2}{4Z_T}\sin^2\theta\right) \\ j\left(\frac{\cos^2\theta}{Z_T} - \frac{4Z_T\sin^2\theta}{Z_C^2}\right) & \left(\frac{Z_C}{4Z_T}+\frac{Z_T}{Z_C}\right)\sin 2\theta \end{bmatrix} \tag{8}$$

Figure 2. The ideal simulated scattering parameters $|S_{11}|$ and $|S_{22}|$ of the impedance matching circuit between 75 Ω and 100 Ω.

In Equation (8), we set $Z_C = Z_e + Z_o$. By solving Equation (8), the following relations are deduced:

$$\tan^2\theta \pm 2\tan\theta \left(\frac{Z_C}{4Z_T} + \frac{Z_C}{Z_T}\right) - \left(1 + \frac{Z_1}{Z_2}\right) \tag{9}$$

$$\tan^2\theta \pm 2\tan\theta \left(Z_1 + \frac{Z^2_1}{2Z_2}\right)\frac{4Z_T}{Z_C^2} - \frac{4Z^2_T}{Z_C^2} \tag{10}$$

For the MTSS to operate at four bands, the system of Equations (9) and (10) must have four distinct solutions, namely $\theta_1, \theta_2, \theta_3,$ and θ_4. These represent the electrical lengths corresponding to the four operating frequencies f_1, $f_2, f_3,$ and f_4. Consequently, Equation (9) must be identical to Equation (10), meaning their coefficients must be equal. From this condition, the following equations are obtained:

$$Z_1 = \frac{Z_C^3}{8Z_T^2} \tag{11}$$

$$Z_2 = \frac{Z_C^5}{8Z_T^2(4Z_T^2 - Z_C^2)} \tag{12}$$

$$\tan\theta = \pm\sqrt{\frac{4Z_T^2}{Z_C^2} + \frac{(Z_C^2 + 4Z_T^2)^2}{16Z_T^2 Z_C^2} \pm \frac{Z_C^2 + 4Z_T^2}{4Z_T Z_C}} \tag{13}$$

From Equation (13), we deduce:

$$\theta_1 = \text{Arctan}\left[\sqrt{\frac{4Z_T^2}{Z_C^2} + \frac{(Z_C^2 + 4Z_T^2)^2}{16Z_T^2 Z_C^2} - \frac{Z_C^2 + 4Z_T^2}{4Z_T Z_C}}\right] \tag{14}$$

$$\theta_2 = \text{Arctan}\left[\sqrt{\frac{4Z_T^2}{Z_C^2} + \frac{(Z_C^2 + 4Z_T^2)^2}{16Z_T^2 Z_C^2} + \frac{Z_C^2 + 4Z_T^2}{4Z_T Z_C}}\right] \tag{15}$$

$$\theta_3 = \pi - \theta_2 \tag{16}$$

$$\theta_4 = \pi - \theta_1 \tag{17}$$

From Equations (16) and (17), the following relations are obtained:

$$\frac{f_2}{f_1} = \frac{\theta_2}{\theta_1} \tag{18}$$

$$\frac{f_3}{f_2} = \frac{\pi}{\theta_2} - 1 \tag{19}$$

$$\frac{f_4}{f_1} = \frac{\pi}{\theta_1} - 1 \tag{20}$$

Thus, based on the derived equations, MTSS can be designed.

Next, we present an illustrative example of designing an impedance-matching circuit between 75Ω and 100Ω at four frequency bands, utilizing the proposed MTSS. It assumed that the first and final frequencies are $f_1 = 1$ GHz and $f_4 = 4$ GHz, respectively. The process of design includes the following steps. First of all, we calculate the characteristic impedance Z_T of the quarter-wavelength transmission line for matching between 75Ω and 100Ω, $Z_T = \sqrt{75.100} = 86.6\Omega$. Next, the quarter-wavelength transmission line Z_T is replaced by the proposed MTSS. Parameters of the proposed MTSS are calculated by applying the closed-form equations (11)–(20). θ_1 is determined by using Equation (20), $\theta_1 = 36^o$. By substituting θ_1 and Z_T to Equation (14), Z_C is given as 120Ω. By using Equations (15) and (18), we obtain $f_2 = 1.965$ GHz. From Equation (19), f_3 is calculated as 3.035 GHz. Impedances Z_1 and Z_2 are determined from Equation (11) and (12), $Z_1 = 28.8\Omega$, $Z_2 = 26.6\Omega$.

Finally, the impedance matching circuit is simulated to verify the calculation method. Figures 2 and 3 illustrate the ideal simulated parameters $|S_{11}|$, $|S_{22}|$, and $|S_{21}|$ of the circuit.

In Fig. 2, it can be observed that the reflection coefficients $|S_{11}|$ and $|S_{22}|$ exhibit identical responses and reach their minimum points at the four designed frequencies 1, 1.965, 3.035, and 4, with values lower than −53 dB. Additionally, Fig. 3 shows that the transmission coefficient $|S_{21}|$ approaches its maximum value of 0 dB at these four design frequencies. These results indicate that the impedance-matching circuit performs effectively, confirming the validity of the design method. The following section will present the design approach for a quad-band RRC based on the proposed MTSS.
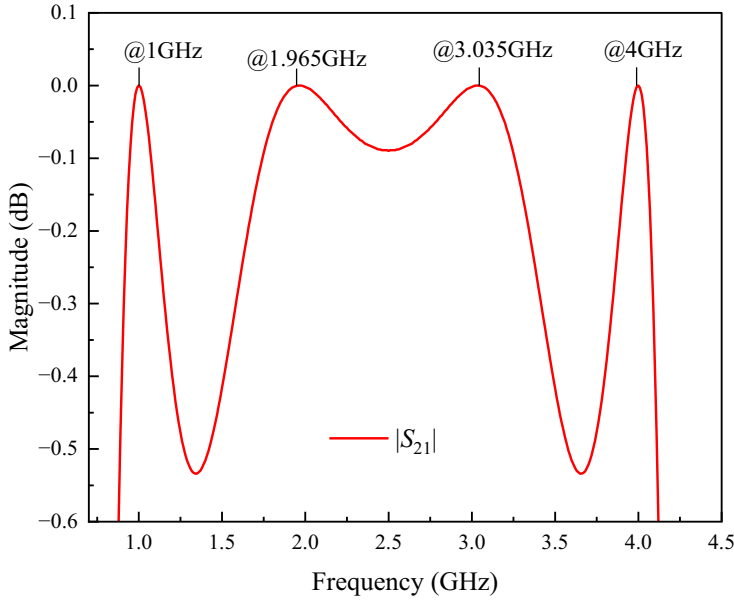
Figure 3. The ideal simulated scattering parameter $|S_{21}|$ of the impedance matching circuit between 75 Ω and 100 Ω.
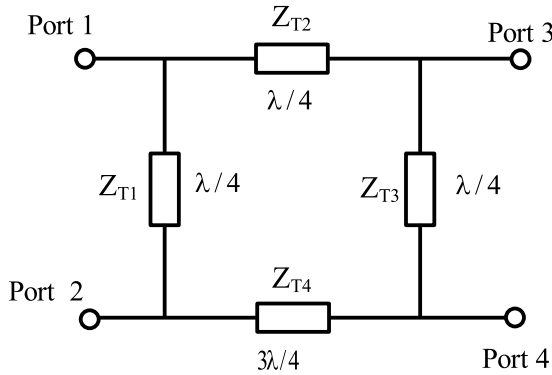
Figure 4. The conventional single-band rat-race coupler [29].

Figure 5. The proposed quad-band RRC.
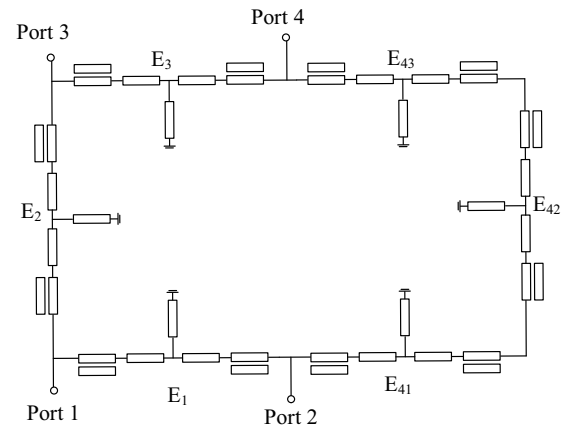
Design method of quad-band RRC

The conventional single-band RRC is presented in Fig. 4 [29].

Figure 4 illustrates a conventional single-band RRC, in which transmission lines are connected to form a circular or square ring. The RRC consists of four ports, including input, output, coupled, and isolated ports. In the RRC, three transmission lines with characteristic impedances Z_{T1}, Z_{T2}, and Z_{T3} are quarter-wavelength (λ/4) lines, and one transmission line with characteristics impedance Z_{T4} is a three-quarter-wavelength (3λ/4) line. All of the transmission lines have the same characteristics as follows:

$$Z_{T1} = Z_{T2} = Z_{T3} = Z_{T4} = Z_T = Z_0\sqrt{2}\,\Omega \qquad (21)$$

where $Z_0 = 50$ Ω.

A proposed quad-band RRC is depicted in Fig. 5. To design the quad-band RRC, the quarter-wavelength transmission lines Z_{T1}, Z_{T2}, and Z_{T3} in the conventional RRC are replaced by the proposed MTSS blocks, which are, respectively, symbolized as E_1, E_2, and E_3. Since the transmission line Z_{T4} has an electrical length of 3λ/4, it is divided into three quarter-wavelength transmission lines with the characteristic impedance Z_{T4}. Then, these three quarter-wavelength transmission lines are replaced by MTSS blocks E_{41}, E_{42}, and E_{43}.

Next, the design constraints of the proposed quad-band RRC are analyzed. When the characteristic impedance of a transmission line is too high or too low, the line width becomes excessively narrow or wide. A narrow line is challenging to fabricate, whereas a wide line significantly increases transmission loss. Therefore, an important design constraint is related to the standard PCB technology, which requires all characteristic impedances Z_1 and Z_2 of the circuit to be in the range from 15 Ω to 120 Ω. From Equations (11) and (12), the following conditions are deduced:

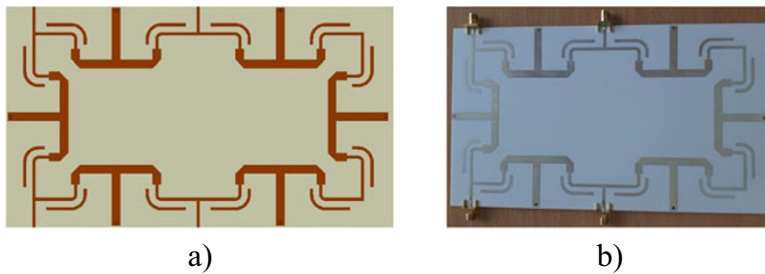$$15\Omega \le \frac{Z_C^3}{8Z_T^2} \le 120\Omega \qquad (22)$$

$$15\Omega \le \frac{Z_C^5}{8Z_T^2(4Z_T^2 - Z_C^2)} \le 120\Omega \qquad (23)$$

Solving the system of inequalities (22) and (23) with the condition $Z_T = 70.71$, we obtain

$$92.7\Omega \le Z_C \le 120.9\Omega \qquad (24)$$
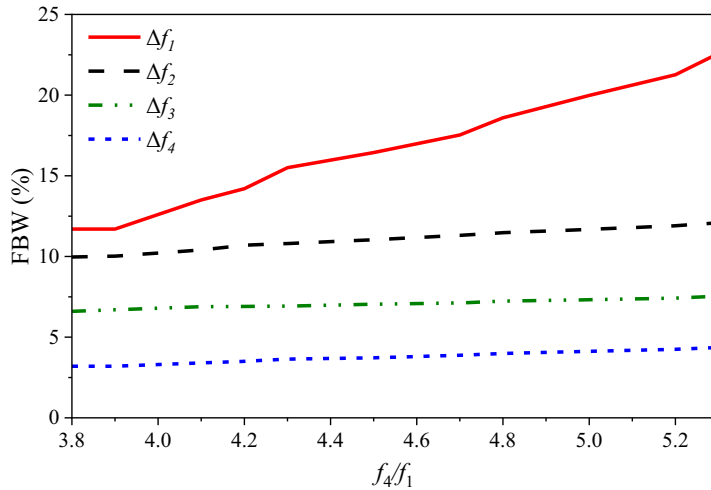
Figure 6. The dependence of four bandwidths of the quad-band RRC on the frequency ratio f_4/f_1.

a)   b)

Figure 7. (a) Layout and (b) photograph of the fabricated quad-band RRC.

By substituting condition (24) into Equations (14) and (15), the following conditions are derived:

$$28.13^o \leq \theta_1 \leq 38.12^o \tag{25}$$

$$68.66^o \leq \theta_2 \leq 71.37^o \tag{26}$$

By substituting Equation (25) into Equation (20), and Equation (26) into Equation (19), we have

$$3.72 \leq \frac{f_4}{f_1} \leq 5.39 \tag{27}$$

$$1.52 \leq \frac{f_3}{f_2} \leq 1.62 \tag{28}$$

Thus, from the above analysis, it can be concluded that the proposed quad-band RRC can operate at four operating bands, provided that the condition $f_4/f_1 \leq 5.39$ is satisfied. This constraint ensures the feasibility of fabricating the quad-band RRC using conventional PCB technology.

From the design equations presented earlier, it also can be seen that when f_1 and f_4 are selected, the frequencies f_2 and f_3 are also determined based on the values of f_1 and f_4. Next, the dependence of the four fractional bandwidths (FBWs) of the quad-band RRC, namely Δf_1, Δf_2, Δf_3, and Δf_4 on the frequency ratio f_4/f_1, is investigated. The bandwidth is defined as the range where $|S_{11}|$ is less than −15 dB. Figure 6 illustrates the simulated dependence of these four FBWs on the frequency ratio f_4/f_1.

From Fig. 6, it can be observed that as the frequency ratio f_4/f_1 increases, the FBW of the first band (Δf_1) exhibits a significant upward trend, indicating a notable expansion in bandwidth. The second band (Δf_2) also shows a moderate increase, though with a much slower rate compared to Δf_1. Meanwhile, the third (Δf_3) and fourth (Δf_4) bands remain nearly constant with minor variations, implying minimal dependence on the frequency ratio f_4/f_1. These trends highlight the impact of the frequency ratio f_4/f_1 on the four FBWs of the proposed quad-band RRC.

Finally, the process of designing a quad-band RRC includes the following steps:

1. Separate the conventional RRC into $\lambda/4$ transmission lines with the same characteristic impedance, $Z_T = 70.71\Omega$. The $3\lambda/4$ transmission line is separated into three $\lambda/4$ transmission lines.
2. Replace the quarter-wavelength transmission lines with equivalent MTSS blocks. Parameters of the MTSS are calculated as below.
   2.1. Select the minimum and maximum operating frequencies, f_1 and f_4, these frequencies must satisfy the condition (27).
   2.2. From Equation (20), determine the electrical length θ_1.
   2.3. Substitute Z_T and θ_1 into Equation (14), then calculate the value of Z_C.
   2.4. From Equation (15), determine the value of θ_2.
   2.5. Use Equations (18) and (19) to calculate operation frequencies f_2 and f_3.
   2.6. Determine the characteristic impedances Z_1 and Z_2 using Equations (11) and (12).

Experimental validation

For further demonstration, a quad-band RRC was designed, fabricated, and tested. The circuit was fabricated using a Rogers
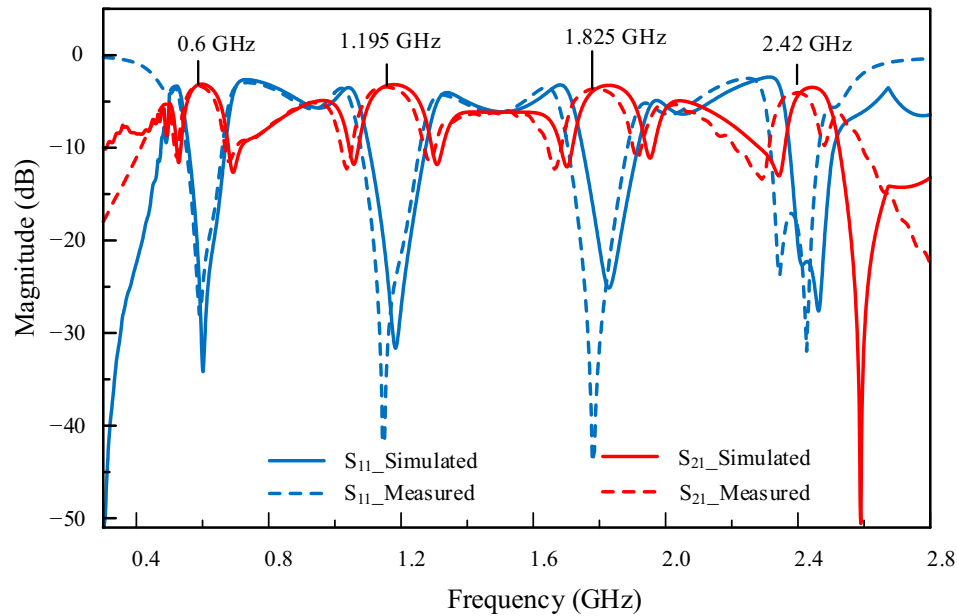
Figure 8. Measured and simulated parameters S_{21} and S_{11} of the proposed quad-band RRC.
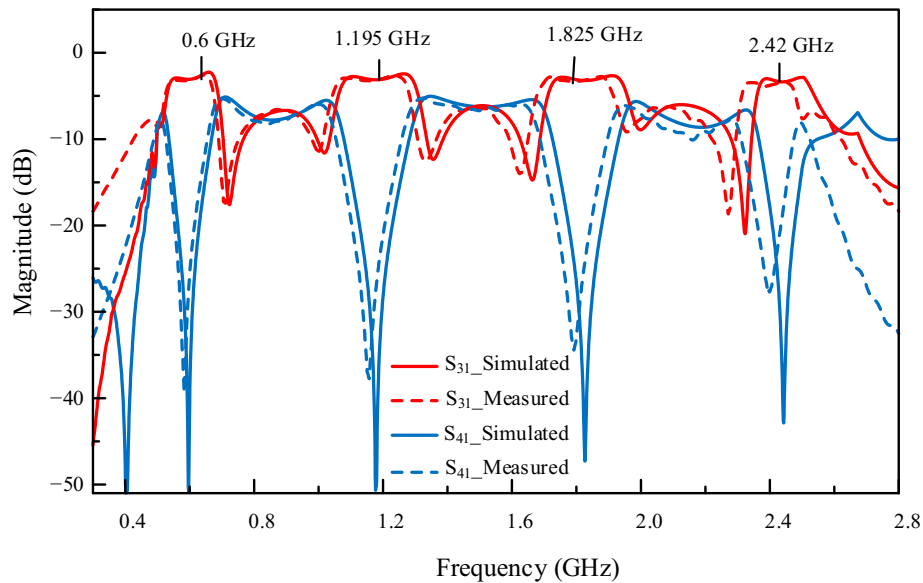
Figure 9. Measured and simulated parameters S_{31} and S_{41} of the proposed quad-band RRC.

RO4003C substrate, which has a relative dielectric constant of 3.55, a thickness of 0.813 mm, and a loss tangent of 0.0027.

Applying the design procedure presented in the previous section, the parameters of the scheme are calculated. Firstly, we choose frequencies $f_4 = 2.45$ GHz and $f_1 = 0.6$ GHz. Then, these frequencies are substituted into Equation (20), and the electrical length θ_1 is defined as $\theta_1 = 35.4°$. From Equations (14) and (15), the values of Z_C and θ_2 are computed as $Z_C = 99.6$ Ω and $\theta_2 = 70.6°$. From there, $Z_e = 51$ Ω and $Z_o = 48.6$ Ω are chosen. From Equations (18) and (19), the operating frequencies f_2 and f_3 are defined as $f_2 = 1.196$ GHz, $f_3 = 1.853$ GHz. Substituting the values of Z_C and Z_T into Equations (11) and (12), we have $Z_1 = 24.7$ Ω and $Z_2 = 24.3$ Ω. The selected frequency bands 0.6, 1.196, 1.853, and 2.45 GHz correspond to various practical applications: 0.6 GHz

for low-frequency wireless communication systems such as LTE Band 71 (600 MHz), which is currently used to provide extended coverage in 4G and 5G networks; 1.196 GHz for global navigation satellite systems (e.g., Galileo E5b, GPS L5); 1.853 GHz for mobile communication; and 2.45 GHz (ISM band) for WLAN and wireless sensor networks. These bands highlight the versatility of the proposed design for modern communication systems.

Figure 7 shows the layout and fabricated prototype of the proposed quad-band RRC. A Vector Network Analyzer is employed to measure the scattering parameters of the fabricated prototype.

Simulated and measured performance of the designed quad-band RRC are presented in Figs. 8–11. The performance results demonstrate the presence of four passbands centered at 0.6, 1.195,
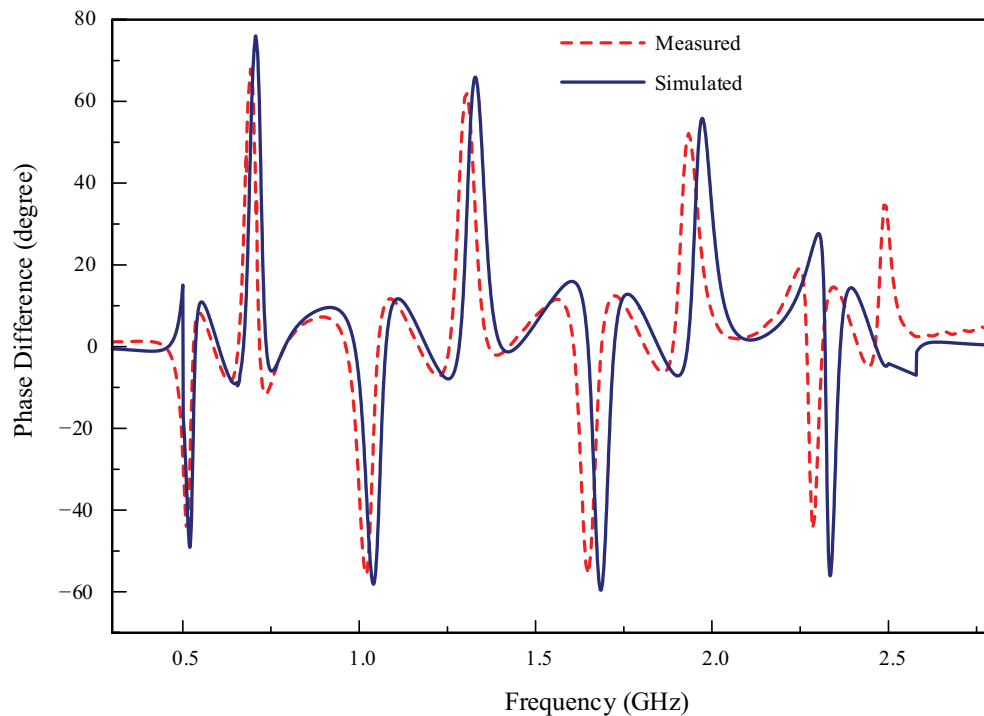
Figure 10. Simulated and measured phase difference between S_{21} and S_{31} of the proposed quad-band RRC.
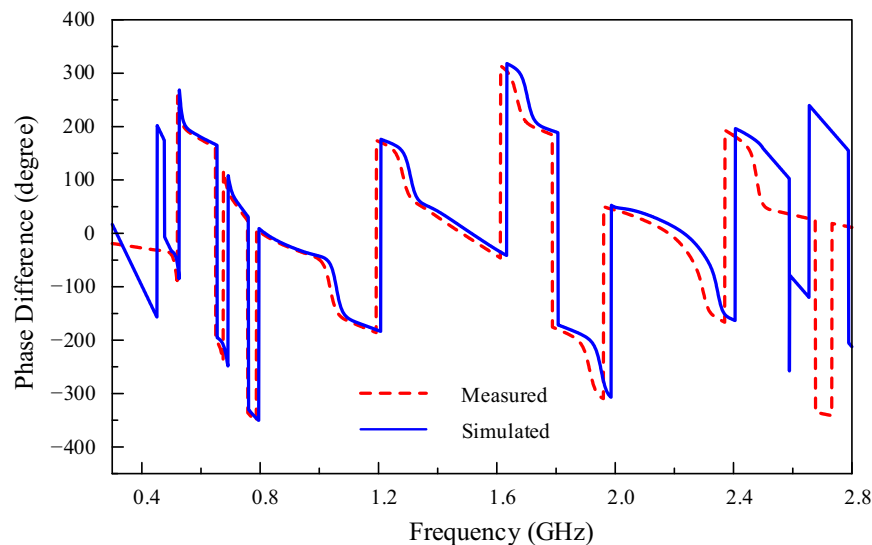
Figure 11. Simulated and measured phase difference between S_{24} and S_{34} of the proposed quad-band RRC.

1.825, and 2.42 GHz. There is a slight shift in the center frequencies of each band, which becomes more pronounced at higher frequencies. This shift is primarily attributed to transmission line discontinuities, including T-junction and bend discontinuities. Additionally, at higher frequencies, the shorter wavelength increases the model's sensitivity to etching inaccuracies, which can affect overall performance. Nevertheless, within the considered frequency range, the proposed model exhibits reliable performance, as validated by both simulation and experimental results. The results suggest that impedance mismatches caused by additional junctions in the proposed circuit have a limited impact within the studied range. However, this behavior may vary if the operating

frequency range is extended, and further investigation is required to fully assess the impact under such conditions.

Figure 8 shows that the measured insertion losses $|S_{21}|$ at the four operating frequencies 0.6, 1.195, 1.825, and 2.42 GHz are 3.18, 3.03, 3.14, and 3.53 dB, respectively. Thus, compared to the ideal 3 dB level, the additional insertion loss is less than 0.53 dB. Meanwhile, the measured input return loss $|S_{11}|$ is better than 21.75 dB at all four central operating frequencies.

Figure 9 describes the measured and simulated $|S_{31}|$ and $|S_{41}|$ parameters of the proposed quad-band RRC. The simulated and measured results show a close agreement. From the graph of Fig. 9, the measured insertion loss $|S_{31}|$ at four operating bands is lower

Table 1. Comparison performance of the proposed quad-band RRC and other reported works

Ref.	f (GHz)	Mat.	Typ.	Tactic	IRL (dB)	IS (dB)	IL (dB)	PD (°)	FBW (%)	Size ($\lambda_g \times \lambda_g$)
[25]	0.9/1.55/2.017/2.55	Rogers 4003B	Quad-band, RRC	Based on negative refractive index transmission lines	>10	>10	<6.37	NI	NI	NI
[26]	1.45/3.8/4.3/6.3	FR4	Quad-band, RRC	Using LODR backed with CDSR	>18.2	>30	<6.3	<8	NI	0.5×0.7
[31]	0.7/1.6/4.32/5.1	Taconic TLY − 5	Quad-band, BLC	Using coupled line, open stubs	>18.18	>17.92	<4.83	<7	28.6/5/ 1.6/2	0.2×0.2
[32]	1/6.16	NI	Dual-band, RRC	Using transmission lines, defected ground structure	>20	>20	NI	<30	NI	0.26×0.264
[30]	1.5/2.4/3.5/4.2	Rogers 5870	Quad-band, BLC	Using an optimized compensation technique	>16.2	>17.7	<4	<2	6.3/5.8/ 1.1/9.3	0.5×0.53
This work	0.6/1.195/ 1.825/2.42	Rogers 4003C	Quad-band, RRC	Using coupled lines, transmission lines, and short stubs	>21.75	>21.6	<4.4	<6.7	10.5/7.8/4.7/2.8	0.46×0.8

than 4.4 dB. Meanwhile, the measured isolation level ($|S_{41}|$) is higher than 21.6 dB.

In-phase response of the proposed quad-band RRC is depicted in Fig. 10. The detailed data indicate that at the four operating frequencies 0.6, 1.195, 1.825, and 2.42 GHz, the phase differences $\angle S_{21} - \angle S_{31}$ are 3.45º, 4.56º, 2.58º, and 1.3º, respectively. Figure 11 illustrates the out-phase responses $\angle S_{24} - \angle S_{34}$ of the RRC. The results show that at four operating frequencies, the phase differences are within 180º ± 6.7º.

Finally, to evaluate the effectiveness of the design approach, the measured performance of the proposed quad-band RRC is compared with other reported works. Comparison results are listed in Table 1.

In Table 1, NI indicates no information; PD is the phase difference; IRL, IS, and IL denote input return loss, isolation, and insertion loss at the four operating frequencies, respectively; BLC is the branch line coupler; λ_g is the guided wavelength at frequency f_1; and FBW is the fractional bandwidth. The FBW is defined as the frequency range where the amplitude imbalance between the two output ports remains within 1 dB for both the proposed quad-band RRC and [30], whereas for [31], it is within 1 dB for the first two bands and 1.5 dB for the last two bands.

Compared to the previously published works [25, 30–32], the proposed quad-band RRC exhibits a significant improvement in isolation, return loss, and insertion loss performance. Specifically, it achieves an isolation level exceeding 21.6 dB, return losses greater than 21.75 dB, and an insertion loss of less than 4.4 dB at four operating frequencies. Although the circuit in [26] achieves better isolation, it exhibits a high insertion loss of up to 6.3 dB and significant phase deviation. Moreover, the proposed RRC design is simpler than those presented in [25, 26], as it features a planar structure, does not use lumped elements, and relies solely on coupled lines, transmission lines, and short stubs. Meanwhile, the quad-band RRC in [25] utilizes negative refractive index transmission lines with MIM capacitors and inductors, while the circuit in [26] employs a laterally offset dual-ring (LODR) resonator backed by concentric dual-split-ring (CDSR) slots and is implemented in a two-layer structure. Thus, these comparisons validate the advantages of the proposed design method. However, despite these benefits, the proposed circuit also presents some drawbacks. The main drawback is its relatively large size compared to the circuits listed in Table 1. This size increase represents a trade-off for achieving a simpler structure and improved performance. In addition, the use of multiple cascaded $\lambda/4$ transmission line sections introduces another potential limitation. At higher frequencies, the multiple junctions between these sections can cause impedance mismatches, leading to undesired reflections, signal loss, or distortion. To mitigate this issue, further optimization through the use of a low-loss substrate or advanced fabrication techniques could improve performance at higher frequencies.

Conclusions

A novel and simple design method for a quad-band RRC based on the proposed MTSS has been presented. To verify the design method, a quad-band RRC was designed, implemented, and measured. The simulated and measured results show good agreement with the design theory. The measured results indicate that the proposed quad-band RRC provides good performance in terms of return loss, insertion loss, and isolation. The proposed model is currently validated over a limited frequency range, which was selected to meet the requirements of the intended applications. In future work, the proposed model will be designed for higher frequencies and applied to various circuit configurations, including Wilkinson power dividers and branch-line couplers. Additionally, circuits with unequal power split ratios will be developed to investigate further use cases.

References

1. **Gruszczynski S and Wincza K** (2012) Broadband rat-race couplers with coupled-line section and impedance transformers. *IEEE Microwave and Wireless Components Letters* **22**, 22–24. https://doi.org/10.1109/LMWC.2011.2177649.
2. **Zheng Y, Wang W, Yang Y and Wu Y** (2020) Single-layer planar wideband rat-race coupler using a shorted parallel-coupled multi-line section. *IEEE Transactions on Circuits and Systems II: Express Briefs* **67**, 3053–3057.
3. **Ahn HR and Tentzeris MM** (2019) Compact and wideband general coupled-line ring hybrids (GCRHS) for arbitrary circumferences and arbitrary power-division ratios. *IEEE Access* **7**, 33414–33423. https://doi.org/10.1109/ACCESS.2019.2902852.
4. **Tseng CH and Chang CL** (2012) A rigorous design methodology for compact planar branch-line and rat-race couplers with asymmetrical T-structures. *IEEE Transactions on Microwave Theory and Techniques* **60**, 2085–2092. https://doi.org/10.1109/TMTT.2012.2195019.
5. **Tolin E, Bahr A and Vipiana F** (2020) Miniaturized and reconfigurable rat-race coupler based on artificial transmission lines. *IEEE Microwave and Wireless Components Letters* **30**, 375–378. https://doi.org/10.1109/LMWC.2020.2972738.
6. **Jianzhong G and Xiaowei S** (2005) Miniaturization and harmonic suppression rat-race coupler using C-SCMRC resonators with distributive equivalent circuit. *IEEE Microwave and Wireless Components Letters* **15**, 880–882. https://doi.org/10.1109/LMWC.2005.859980.
7. **Nie W, Luo S, Guo Y and Fan Y** (2014) Miniaturized rat-race coupler with harmonic suppression. *IEEE Microwave and Wireless Components Letters* **24**, 754–756. https://doi.org/10.1109/LMWC.2014.2350253.
8. **Park MJ and Lee B** (2011) Design of ring couplers for arbitrary power division with 50 Ω lines. *IEEE Microwave and Wireless Components Letters* **21**, 185–187. https://doi.org/10.1109/LMWC.2011.2112341.
9. **Chaudhary G and Jeong Y** (2016) Arbitrary power division ratio rat-race coupler with negative group delay characteristics. *IEEE Microwave and Wireless Components Letters* **26**, 565–567. https://doi.org/10.1109/LMWC.2016.2585561.
10. **Chi PL and Ho KL** (2014) Design of dual-band coupler with arbitrary power division ratios and phase differences. *IEEE Transactions on Microwave Theory and Techniques* **62**, 2965–2974. https://doi.org/10.1109/TMTT.2014.2364218.
11. **Tseng CH, Mou H, Lin C and Chao CH** (2016) Design of microwave dual-band rat-race couplers in printed-circuit board and GIPD technologies. *IEEE Transactions on Components, Packaging, and Manufacturing Technology* **6**, 262–271. https://doi.org/10.1109/TCPMT.2015.2507371.
12. **Zhang H and Chen KJ** (2009) Design of dual-band rat-race couplers. *IET Microwaves, Antennas & Propagation* **3**, 514–521. https://doi.org/10.1049/iet-map.2008.0019.
13. **Majeed A and Ashraf M**. (2008) Dual band ring couplers using T and π section. *International Journal of Microwave and Optical Technology* **3**, 460–466.
14. **Chin KS, Lin KM, Wei MY, Tseng TH and Yang YJ** (2010) Compact dual-band branch-line and rat-race couplers with stepped-impedance-stub lines. *IEEE Transactions on Microwave Theory and Techniques* **58**, 1213–1221. https://doi.org/10.1109/TMTT.2010.2046064.
15. **Chen CC, Sim YD and Wu YJ** (2016) Miniaturised dual-band rat-race coupler with harmonic suppression using synthetic transmission line. *Electronics Letters* **52**, 1784–1786. https://doi.org/10.1049/el.2016.2154.

16. **Zhebin W and Park CW** (2012) Multiband pi-shaped structure with resonators for tri-band Wilkinson power divider and tri-band rat-race coupler. IEEE/MTT-S International Microwave Symposium Digest, Canada

17. **Chu QX and Lin F** (2010) A novel tri-band rat-race coupler with T-shape step impedance transformers. *Microwave and Optical Technology Letters* **52**, 1240–1244. https://doi.org/10.1002/mop.25186.

18. **Cheng WG and Ming L** (2015) Compact tri-band rat-race coupler based on novel metamaterial transmission line, Asia-Pacific Microwave Conference (APMC), Nanjing, China.

19. **Wei F, Zhang C-Y, Yue H-J and Shi X-W** (2019) Balanced quad-band bandpass filter with controllable frequencies and bandwidths. *IEEE Access* **7**, 140470–140477. https://doi.org/10.1109/ACCESS.2019.2943704.

20. **Wei F, Yue H-J, Zhang X-H and Shi X-W** (2019) A balanced quad-band BPF with independently controllable frequencies and high selectivity. *IEEE Access* **7**, 110316–110322. https://doi.org/10.1109/ACCESS.2019.2934494.

21. **Abdalla MA and Hu Z** (2018) Design and analysis of a compact quad band loaded monopole antenna with independent resonators. *International Journal of Microwave and Wireless Technologies* **10**, 479–486. https://doi.org/10.1017/S1759078717001453.

22. **Maamria T, Challal M, Benmahmoud F, Fertas K and Mesloub A** (2023) A novel compact quad-band planar antenna using meander-line, multi-stubs, and slots for WiMAX, WLAN, LTE/5G sub-6 GHz applications. *International Journal of Microwave and Wireless Technologies* **15**, 852–859. https://doi.org/10.1017/S1759078722000939.

23. **Keshavarz R, Mohammadi A and Abdipour, A.** (2017) A linearity improved quad-band amplifier based on E-CRLH transmission line. *International Journal of Microwave and Wireless Technologies* **9**, 1603–1610. https://doi.org/10.1017/S1759078717000253.

24. **Althuwayb A** (2021) Design of quad-band rat-race coupler for GSM/WiMAX/WLAN/Satellite Applications. *Radioengineering* **30**, 135–141. https://doi.org/10.13164/re.2021.0135.

25. **Papanastasiou A** (2015) Design and implementation of quad-band microwave devices using the negative refractive index transmission-line technique. Ph.D. dissertation, Dept. of Electrical and Computer Engineering, University of Cyprus, Nicosia, Cyprus, May

26. **Velan S, Kingsly S, Kanagasabai M, Alsath MGN, Panneer SY, and Subbaraj S** (2016) Quad-band rat-race coupler with suppression of spurious pass-bands. *IEEE Microwave and Wireless Components Letters* **26**, 490–492. https://doi.org/10.1109/LMWC.2016.2575017.

27. **Giang NM, Thang LHM, Manh LD and Huong TTT** (2024) A simple design of low-loss quad-band Wilkinson power dividers. *Journal of Electrical Engineering* **75**, 63–71.

28. **Sahu A, Shamaileh KA, Aaen PH and Abu-shamleh SA** (2021) A high-frequency/power ratio wilkinson power divider based on identical/non-identical multi-T-sections with short-circuited stubs. *IEEE Open Journal of Circuits and Systems* **2**, 34–45. https://doi.org/10.1109/OJCAS.2020.3043354.

29. **Pozar DM** (2012) *Microwave Engineering*. New York: Wiley

30. **Piazzon L, Saad P, Colantonio P, Giannini F, Andersson K and Fager C** (2012) Branch-line coupler design operating in four arbitrary frequencies. *IEEE Microwave and Wireless Components Letters* **22**, 67–69. https://doi.org/10.1109/LMWC.2011.2181349.

31. **Guoan W, Shihao Q, Wenguang L, Baoquan H and Lamin Z** (2021) A quad-band branch line coupler with high frequency ratio. *IEICE Electronics Express* **19**, 1–5.

32. **Liang J-G, Zhang X-C and Liao Z-H** (2018) Novel design of a dual-band rat-race coupler with large power division ratio, *International Conference on Microwave and Millimeter Wave Technology (ICMMT)*, Chengdu, China, 1–3.

Nguyen Minh Giang was born in 1985 in Thai Nguyen, Vietnam. He received a Ph.D. degree in electronics engineering from Irkutsk National State Technical University, Russia, in 2018. He is currently a senior lecturer in the Faculty of Radio-Electronic Engineering at Le Quy Don Technical University, Vietnam. His current research interests focus on the design of broadband and multi-band passive microwave components, and microwave technologies.

Le Ho Manh Thang received his Diploma in telecommunications engineering in 2024 from the Le Quy Don Technical University. His current research interests include microwave technologies, and the design of broadband and multi-band passive microwave components such as power dividers, filters, couplers, and others.

Tran Thi Thu Huong received the B.E. degree in electrical and electronic engineering and the M. E. degree in electronics engineering from Le Quy Don Technical University, Ha Noi, VietNam in 2009 and 2013, respectively. She received the Ph.D. degree from The University of Electro-Communications, Tokyo, Japan in 2017. Her current research interests are in the field of radio and microwave technologies.